In situ bend testing of niobium-reinforced alumina nanocomposites with and without single-walled carbon nanotubes

Katherine E. Thomson [a], Dongtao Jiang [a], Joseph A. Lemberg [b], Kurt J. Koester [b], Robert O. Ritchie [b], Amiya K. Mukherjee [a],*

[a] *Department of Chemical Engineering and Materials Science, University of California, Davis, United States*
[b] *Lawrence Berkeley Laboratory and Department of Materials Science and Engineering, University of California, Berkeley, United States*

Abstract

Alumina-based nanocomposites were fabricated and consolidated via spark plasma sintering. The effect of single-walled carbon nanotube (SWCNT) and niobium additions to nanocrystalline alumina was examined by in situ bend testing. The addition of 10 vol.% niobium to nanocrystalline alumina provided substantial improvement of fracture toughness ($6.1\,\mathrm{MPa\,m^{1/2}}$)—almost three times that of nanocrystalline alumina. Observation of cracks emanating from Vickers indents, as well as bend specimen fracture surfaces, reveal the operation of ductile phase toughening in the Nb–Al_2O_3 nanocomposites. Further addition of 5 vol.% SWCNTs to the 10 vol.%Nb–Al_2O_3 revealed a more porous structure and less impressive fracture toughness—having an indentation and bend fracture toughness of $2.9\,\mathrm{MPa\,m^{1/2}}$ and $3.3\,\mathrm{MPa\,m^{1/2}}$, respectively.
Published by Elsevier B.V.

Keywords: Spark plasma sintering (SPS); Al_2O_3; Nb; Nanocomposites; Carbon nanotubes; Fracture toughness

1. Introduction

Recently, controversy has grown over whether the addition of carbon nanotubes to nanocrystalline alumina (Al_2O_3) benefits the brittle ceramic's mechanical properties, specifically its fracture toughness [1–4]. However, it is clear that the addition of carbon nanotubes can add electrical and thermal conductivity to an otherwise insulating material. The carbon nanotubes that primarily exist at the grain boundaries of alumina provide an effective matrix of conducting pathways [5]. If the fracture toughness can be improved, ceramic matrix composites (CMCs) hold great promise for use in structural and load bearing applications. CMCs possess superior chemical inertness, higher hardness, and lower densities than metals and their alloys. Furthermore, CMCs with nanocrystalline matrices have superior strength and hardness properties over their microcrystalline counterparts. Unfortunately, the monolithic fracture toughness of the nanocrystalline ceramic matrices is significantly less than those in the microcrystalline regime. For example, microcrystalline alumina has an intrinsic fracture toughness of $\sim3.3\,\mathrm{MPa\,m^{1/2}}$—as compared to about $2.3\,\mathrm{MPa\,m^{1/2}}$ for nanocrystalline alumina [6].

The addition of ductile phases such as metals to ceramic matrices has been proven to be an effective toughening mechanism [7]. Energy is dissipated from the propagating crack through two different phenomena: crack blunting at the ductile particle and/or absorption of energy through the deformation of the ductile phase. Both phenomena relieve the stress field around the crack tip.

The addition of fibers to a brittle ceramic matrix can improve the fracture toughness by means of fiber bridging. Toughening is achieved when the fibers either shed load from the crack tip while remaining intact, debonding between the fiber and the matrix followed by fiber pullout, and/or fracture of the individual fibers followed by energy absorption through pullout of the broken fiber. Another toughening mechanism that is quite common in fiber-reinforced composites is crack deflection [8]. This occurs in situations in which the fiber is significantly stronger than the matrix and the fiber is favorably oriented as to allow for the crack propagation direction to proceed away from the axis of highest

* Corresponding author.
E-mail address: akmukherjee@ucdavis.edu (A.K. Mukherjee).

stress. Commonly, the crack deflects to a less efficient cleavage plane directed by the longitudinal direction of the fiber. This scenario leads to increased fracture energy through increased surface area and lower driving forces due to the reduced resolve normal stresses at the crack tip [9].

The present work examines the mechanical properties of nanocrystalline alumina reinforced with niobium with and without single-walled carbon nanotubes (SWCNTs). Mechanical bend testing conducted within an SEM, as well as indentation testing, was used to reveal the extent of ductile phase toughening produced by the addition of 10 vol.% niobium to nanocrystalline alumina. In addition, these same methods were used to study the nature and extent of failure mechanisms present when 5 vol.% SWCNTs was introduced to the Nb-Al_2O_3 system.

2. Experimental procedures

2.1. Powder processing of Nb/alumina and Nb/SWCNT/alumina nanocomposite powders

The following powders were mixed by hand prior to high-energy ball milling (HEBM): as-received alumina powder (α and γ phases, 45 nm, Baikowski International Corp.), the appropriate amount of 90 wt.% Nb (99.85% purity, 74 μm, Goodfellow)-10 wt.% Al (99.5% purity, 45 μm, Johnson Matthey Electronics) alloy to yield a 10 vol.%Nb/alumina composition, and 1 wt.% polyvinyl alcohol (PVA). Aluminum was added to reduce the surface oxide of the niobium particles and PVA was added to prevent severe powder agglomeration. This powder mixture was placed in a tungsten-carbide (WC) vial and HEBMed for 24 h using one WC ball. The composite powder was heat treated (at 350 °C for 3 h in vacuum) to remove the PVA before further processing was performed.

The Nb/alumina composite powder was ultrasonicated for 15 min in 500 ml of ethanol. The slurry was then added to a polypropylene bottle with 280 g (~1/3 by volume) of zirconia ball media and wet-milled (130 rpm) for 24 h. For the composites containing carbon nanotubes, the appropriate amount of SWCNTs (~90% purity, Carbon Nanotechnologies Inc., Texas) was weighed out. The SWCNTs were produced by the HiPco process and had diameters of 0.8–1.7 nm and length of up to 1 μm. During final minutes of the previously mentioned wet milling, 8 ml of Nanosperse (an organic surfactant made by NanoLab) was stirred into 150 ml of DI water. The SWCNTs were added to this solution and ultrasonicated for 5 min. The wet-milled slurry was slowly added to the dispersed carbon nanotube solution while ultrasonicating was added back into the polypropylene bottle and wet-milled for an additional 24 h.

In both cases, the Nb/alumina and Nb/SWCNT/alumina slurries were taken off the wet-mill, ball media separated, sieved through a 150 μm mesh, and placed into medium sized glass beaker. A magnetic stir bar was added and the slurry was dried on a stirring hotplate. Once dry, the agglomerates were broken up with a mortar and pestle and sieved through 150 μm mesh. In the case of the Nb/SWCNT/alumina powders, the dispersant was baked off at 450 °C for 4 h.

2.2. Spark plasma sintering (SPS)

Consolidation was performed under vacuum in the Dr. Sinter 1050 SPS machine. The following processing parameters were used: 105 MPa of applied pressure, and "on" pulse of 12 cycles of 2 ms each and a "off" interval between pulses of 2 cycles, a maximum pulse settings of 5000 A and 10 V, and a pressure of 105 MPa. An optical pyrometer was used to measure temperature and a heating rate of 125 K/min was used from room temperature to 600 °C. From 600 °C to the desired final set point (1200–1300 °C in this study), heating rates ranged from 150 K/min to 233 K/min. SPS consolidation yielded fully dense (98 + %TD) samples fit for microstructural characterization and mechanical testing. Density was determined via Archimedes method and consolidated samples had dimensions of 19 mm in diameter and 3–4 mm in thickness.

2.3. Mechanical testing and characterization

Samples were polished to 0.5 μm surface finish and cut into beams having dimensions of 3 mm × 4 mm × 19 mm. The beam samples were pre-notched using a diamond saw, followed by an automated razor blade with 1 um diamond paste to (a/W) ratio of 0.25–0.5. Sample preparation procedures were made in accordance with ASTM STP 1409 presented in reference [10]. The pre-notched beams were three-point bend tested within a Hitachi S-4300SE/N scanning electron microscope using a Gatan Microtest 2000 test assembly. Crack propagation was observed under a 0.55 μm/s loading rate and the breaking load was recorded. The following equations from ASTM Standard E399-90 were used to calculate the nanocomposites' fracture toughness [11]:

$$K_{Ic} = P \frac{S}{(BW^{3/2})} F\left(\frac{a}{W}\right), \quad F\left(\frac{a}{W}\right) =$$

$$3 \frac{\left(\frac{a}{W}\right)^{1/2} \left(1.99 - \left(\frac{a}{W}\right)\left(1 - \left(\frac{a}{W}\right)\right)\left(2.15 - 3.93\left(\frac{a}{W}\right) + 2.7\left(\frac{a}{W}\right)^2\right)\right)}{\left(2\left(1 + 2\left(\frac{a}{W}\right)\right)\left(1 - \left(\frac{a}{W}\right)\right)^{3/2}\right)}$$

where P is the breaking load, S the pin span (in this case 15 mm), B the width, W the height, and a is the notch depth. Fracture surfaces were analyzed in a FEI XL-30 SFEG Scanning electron microscope. For comparison, the fracture toughness of the nanocomposites was calculated using the indentation method using a standard Tukon microhardness tester using a diamond Vickers indenter and 2.28 kN load. A Buehler light microscope and ANALYSIS program was used to measure the cracks emitted from the indentations.

3. Results and discussion

Indents were measured and the hardness and fracture toughness averaged over 10 valid indents. Results from all materials tested are given in Table 1. For comparison, a pure alumina sample (slightly larger grain size of 1.4 μm) was fabricated and tested using identical procedures for a base line comparison. The three-point bend setup is accurate in that it predicted about

Table 1
Summary of data gathered in the Nb–alumina nanocomposites with and without SWCNTs

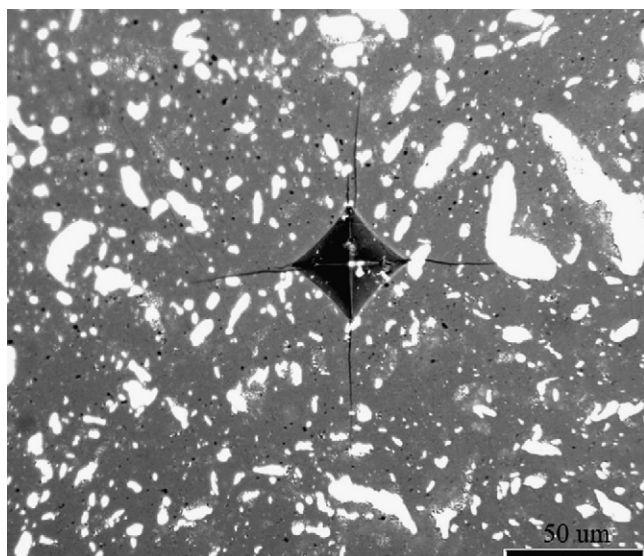| Composition	SPS parameters	Density (% TD)	Grain size	Indentation K_{Ic} (MPa m$^{1/2}$)	Bend K_{Ic} (MPa m$^{1/2}$)	Hardness (GPa)
Al$_2$O$_3$	1300 °C/3 min	99.9	1.4 μm	2.7	3.1	20.9
10%Nb–Al$_2$O$_3$	1150 °C/3 min, 1300 °C/2 min	99.5	250 nm	3.3	6.1	22.9
10%Nb–5%SWCNT–Al$_2$O$_3$	1200 °C/5 min	98.4	580 nm	2.9	3.3	19.3

Fig. 1. Optical micrograph of an indent on 10 vol.%Nb–Al$_2$O$_3$ surface showing the effectiveness of the niobium regions at stopping crack propagation.

Fig. 2. SEM image of 10 vol.%Nb–Al$_2$O$_3$ fracture surface (Au-coated) displaying two modes of failure—particle debonding (arrow) and cleavage fracture. Notch region at bottom of image.

a 3 MPa m$^{1/2}$ fracture toughness—consistent with microcrystalline alumina. The matrix grain size greatly decreases when Nb and/or SWCNTs are added, as frequently observed in CMCs [12,13].

3.1. 10 vol.%Nb–Al$_2$O$_3$ nanocomposites

Indentation method revealed a hardness of 22.9 GPa and fracture toughness of 3.3 MPa m$^{1/2}$ for the 10 vol.%Nb–alumina composite. Observation of the indents made in the 10 vol.%Nb–Al$_2$O$_3$ show that the niobium regions are effective in stopping propagating cracks. Crack blunting can be seen on the right corner of the indent in Fig. 1. This is consistent with ductile phase toughening theory. Clearly, HEBMing technique produces a large size distribution of niobium particles—many much finer but others close to the as-received 74 μm particle size. Residual porosity is also apparent in some regions.

Although stable crack growth was not observed in the in situ bend testing, the K_{1C} value obtained from the breaking load was 6.1 MPa m$^{1/2}$. Analyses of the post-mortem fracture surfaces indicate two distinct failure modes of the niobium particles. Both of which are apparent on the niobium particle in Fig. 2. First, some of the niobium regions completely debonded from the brittle alumina matrix. And in some cases, imprints of the small alumina grains can be seen in the region of debonding. Second, it is apparent that the majority of the niobium particles tended to fracture in a brittle manner that is typical for body-
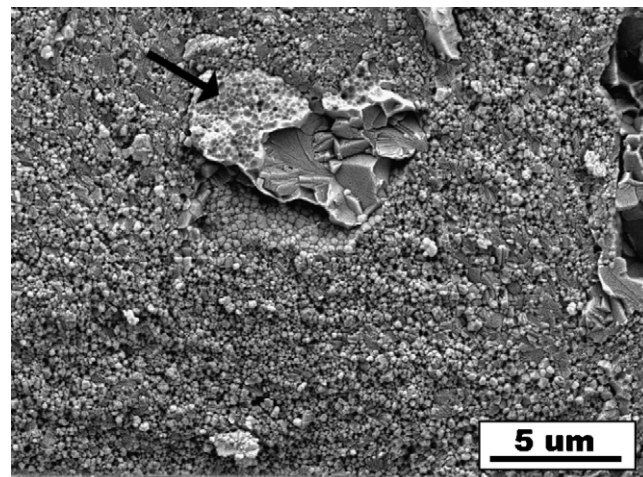
centered cubic and high melting point metals such as niobium. Cleavage fracture and the presence of river lines indicate that the niobium particles ultimately failed without much plasticity. However, the resulting bend fracture toughness of 6.1 MPa m$^{1/2}$ indicate that the niobium regions did indeed absorb some energy from the propagating crack. Since this energy was not used to plastically deform the niobium, the crack propagation resistance is attributed to crack blunting and crack bridging. Such crack-tip shielding toughening mechanisms were also observed by other investigators in Nb/Nb$_3$Al composites [14].

The premise of in situ testing is to directly observe niobium particles bridging the crack wake. Stable crack growth was not observed in any of the V-notched samples. Therefore, a bias-notched sample (the crack grows into an increasing wedge of material and thus a decreasing K-field situation) was produced and tested under identical conditions. Even in this scenario, no stable crack growth was observed. Comparison of the last image taken before fast fracture and the image of the broken sample indicated that the crack that resulted in failure was on the order of a few microns. Thus, any R-curve behavior occurs within the first few microns of crack growth and could not be resolved in this experiment.

3.2. 10 vol.%Nb–5 vol.%SWCNT–Al$_2$O$_3$

Measurement of the cracks emanating from the indents made in 10 vol.%Nb–5 vol.%SWCNT–Al$_2$O$_3$ was much more difficult due to the increased porosity ($\sim$1.5%) and the dark
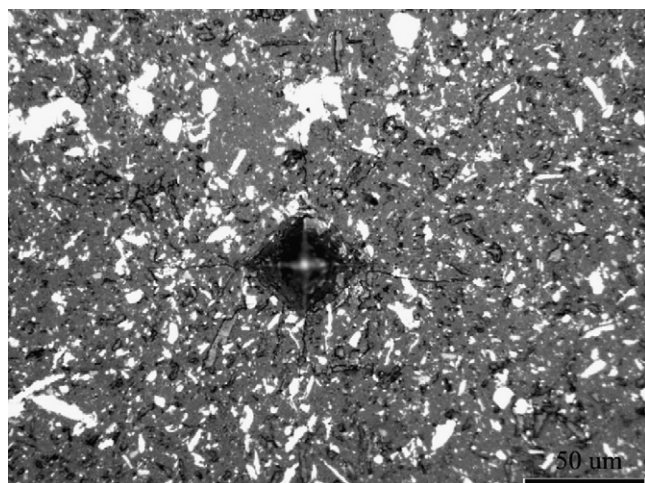
Fig. 3. Optical micrograph of an indent on 10 vol.%Nb–5 vol.%SWCNT–Al$_2$O$_3$ surface.
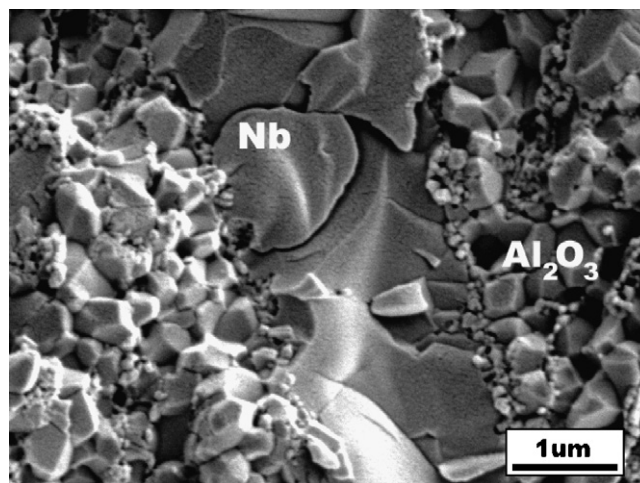

Fig. 4. SEM image of 10 vol.%Nb–5 vol.%SWCNT–Al$_2$O$_3$ fracture surface (Au-coated) revealing similar brittle failure of a niobium particle and carbon nanotubes (appear as small particles) at the alumina grain boundaries.

color of the carbon nanotube agglomerates. Scanning electron microscopy (SEM) analysis revealed that the majority of carbon nanotube agglomerates were sub-micron with sizes ranging from a single nanotube bundle to larger agglomerates with widths of ∼1 μm. A representative indent is shown in Fig. 3. Measurements of the indents revealed a lower hardness (19.3 GPa) and fracture toughness (2.7 MPa m$^{1/2}$) than the 10 vol.%Nb–Al$_2$O$_3$ system. This very small increase in fracture toughness over typical nanocrystalline alumina may be attributed to the increased porosity with the addition of carbon nanotubes or the difficulty in measuring the crack length. It is possible that nanotube agglomerates were mistaken for a continuing crack. This is the disadvantage of using the indentation method to determine the fracture toughness of a composite and the reason for discrepancies in literature. In comparison of Figs. 2 and 3, it appears that the niobium regions played less of a role in stopping the propagating cracks in the system in which the carbon nanotubes were introduced. The reason for this difference is unclear.

The in situ bend testing revealed a fracture toughness of 3.3 MPa m$^{1/2}$. Comparison of both the indentation and bend test fracture toughness of pure alumina and the Nb–CNT–alumina nanocomposite reveals little or no improvement of fracture toughness with the addition of niobium and carbon nanotubes. In fact, the addition of carbon nanotubes appeared to remove any toughening effect of niobium seen in the Nb–Al$_2$O$_3$ system. The porosity around the carbon nanotube agglomerates is thought to be the reason for the negative effect on toughness when 5 vol.% SWCNT is added. Consequently, the more dispersed the carbon nanotubes are the more dispersed the porosity is also. This porosity seems to be unavoidable because of the limitation of SPS temperature due to the presence of carbon nanotubes. A previous work revealed that the structure of carbon nanotubes begin to break down at SPS temperatures above 1150 °C [15]. Thus in order to obtain as dense a specimen as possible, the hold time at 1200 °C was extended to 5 min—resulting in only a 98.5% dense sample.

The fracture surfaces of the 10 vol.%Nb–5 vol.%SWCNT–Al$_2$O$_3$ nanocomposites show a slightly larger grain size than the Nb–Al$_2$O$_3$ system due to the increase in SPS hold time (Fig. 4). The carbon nanotubes are present in the alumina grain boundaries as well as between the niobium particles and the alumina matrix. Agglomerates of carbon nanotubes ranged from tens of nanometers to a few micrometers in width. Similar brittle failure of the niobium particles was also observed this system. The majority of cracks and pores were seen at the alumina–carbon nanotube interfaces and crack bridging was seen in a few circumstances.

4. Summary

Alumina-based nanocomposites containing niobium with and without carbon nanotubes were synthesized with advanced powder processing techniques and consolidated via SPS. The fracture toughness was measured using both indentation and three-point bend techniques. Nanocrystalline alumina has a very low fracture toughness of ∼2.5 MPa m$^{1/2}$. The most toughening occurred when 10 vol.% niobium is added to nanocrystalline alumina—raising the bend fracture toughness to 6.1 MPa m$^{1/2}$. However, when 5 vol.% SWCNTs are added to this system the bend fracture toughness fell to 3.3 MPa m$^{1/2}$. The decrease in fracture toughness is attributed to the increase in porosity in the carbon nanotube-containing nanocomposite—which seems to be unavoidable despite an increase in SPS hold time. The 10 vol.%Nb–Al$_2$O$_3$ system holds promise for load bearing applications. On the other hand, the carbon nanotube-containing system would be ideal if a conductive ceramic without degraded fracture toughness is desired. In situ bend testing was conducted with the premise of observing stable crack growth and obtaining the R-curve of toughened alumina nanocomposites. Even in the bias-notched sample, no stable crack growth was observed. Analysis of the last SEM image taken before catastrophic failure of the 10 vol.%Nb–Al$_2$O$_3$ bias-notched sample suggested that the crack that caused failure was on the order of a few microns. Therefore, if any R-curve behavior exists, it is within the first few microns of crack growth.

K.E. Thomson et al. / Materials Science and Engineering A xxx (2008) xxx–xxx   5

Acknowledgement

References

[1] G.-D. Zhan, J. Kuntz, J. Wan, A.K. Mukherjee, Nat. Mater. 2 (2003) 38–42.
[2] X. Wang, N. Padture, H. Tanaka, Nat. Mater. 3 (2004) 539–544.
[3] S.I. Seung, K.T. Kim, K.H. Lee, C.B. Mo, S.H. Hong, Scripta Mater. 53 (2005) 793–797.
[4] R.W. Siegel, S.K. Chang, B.J. Ash, J. Stone, P.M. Ajayan, R.W. Doremus, L.S. Schadler, Scripta Mater. 44 (2001) 2061–2064.
[5] G.-D. Zhan, A.K. Mukherjee, Int. J. Appl. Ceram. Technol. 1 (2004) 161–171.
[6] R.S. Mishra, A.K. Mukherjee, Mater Sci. Eng. A 301 (97–101) (2001).
[7] W.H. Tuan, R.J. Brook, J. Eur. Ceram. Soc. 6 (1990) 31–37.
[8] H. Suemasu, A. Kondo, K. Itatani, A. Nozue, Compos. Sci. Technol. 61 (2) (2001) 281–288.
[9] J.B. Wachtman, Mechanical Properties of Ceramics, John Wiley & Sons Inc., New York, 1996, pp. 159–218.
[10] J.J. Kubler, ASTM STP 1409, J.A. Salem, G.D. Quinn, M.G. Jenkins, Eds. ASTM (2002).
[11] ASTM Standard E399-90, Standard Test Method for Plane-Strain Fracture Toughness of Metallic Materials, Annual Book of ASTM Standards, vol. 03.01.
[12] Z. Chen, T. Takeda, K. Ikeda, T. Murakami, Scripta Mater. 43 (2000) 1103–1109.
[13] C.L. Mohamed, N. Rahaman, J. Am. Ceram. Soc. 75 (1992) 2056–2065.
[14] C.D. Bencher, A. Sakaida, K.T. Venkateswara Rao, R.O. Ritchie, Metall. Mater. Trans. A 26 (1995) 2027–2033.
[15] D.T. Jiang, K.E. Thomson, J.D. Kuntz, J.W. Ager, A.K. Mukherjee, Scripta Materialia 56 (2007) 959–962.